

Primary Versus Secondary Leptons in the EGRET SNR's

Marco Fatuzzo¹ and Fulvio Melia²

¹*Physics Department, Xavier University, Cincinnati, OH 45207*

²*Physics Department and Steward Observatory, The University of Arizona, AZ 85721*

ABSTRACT

The EGRET supernova remnants (SNR's) are all expanding into nearby dense molecular clouds, powering a shock at the interface where protons and electrons accelerate to relativistic energies. A viable mechanism for the emission of γ -rays in these sources is the decay of neutral pions created in collisions between the relativistic hadrons and protons in the ambient medium. But neutral pion decay alone cannot reproduce the whole high-energy spectrum, particularly below 100 MeV. A pion-decay scenario thus requires a lepton population to "fill in" the lower part of the spectrum via bremsstrahlung emission. This population, however, is constrained by the SNR radio spectrum. Taking our cue from the behavior of Sgr A East, an energetic EGRET SNR at the Galactic center, we here examine the role played in these sources by secondary leptons—electrons and positrons produced in proton-proton scattering events and the ensuing particle cascades. We show that while secondary leptons cannot account for the γ -rays below 100 MeV, they can account for the hard radio spectra observed from the EGRET SNR's. Thus, it appears that both primary and secondary leptons may be important contributors to the overall broadband emission from these sources, but if so, must radiate most of their energy in different parts of the SNR-cloud environment. We show that shock acceleration in dense cores being overtaken by the expanding SNR shell can naturally lead to such a scenario.

Subject headings: acceleration of particles—cosmic rays—Galaxy: center—galaxies: nuclei—radiation mechanisms: nonthermal—supernova remnants

1. Introduction

Several supernova remnants have now been associated with EGRET sources (Esposito et al. 1996; Combi, Romero & Benaglia 1998; Combi et al. 2001). What appears to unify these remnants is their interaction with nearby dense molecular clouds. The EGRET SNR's

also constitute a subset of a larger class of remnants (numbering ~ 20) that produce OH (1720 MHZ) maser emission (Yusef-Zadeh et al. 2003), whose appearance helps to constrain the densities and temperatures of post-shock gas found in these environments. Additionally, magnetic field strengths and orientations may be deduced from Zeeman splitting and polarization studies. All in all, the physical conditions within, and surrounding, these high-energy sources, may be deduced with sufficient precision to model the diffusive particle acceleration thought to be responsible for much of their emissivity (as discussed in §2).

By now, the EGRET SNR's have been observed in radio, infrared, X-rays and γ -rays. These observations provide important clues about the processes at play in these environments. For example, these sources are strong radio emitters (> 100 Jy at 1 GHz) and have spectra that can be significantly harder than those of most SNR's. Additionally, the non-detection of EGRET SNR's at TeV energies (e.g., Buckley et al. 1998; Rowell et al. 2000) sets important constraints on the distribution of energetic particles. Their apparent cutoff at high energy can be understood in terms of the limits placed on effective particle acceleration by the large densities in these environments (Baring et al. 1999). As such, the EGRET SNR's appear to be an ideal class of objects to study shock acceleration and cosmic ray production.

Indeed, the study of gamma-ray production in SNR-cloud environments has been undertaken by several authors. De Jager and Mastichiadis (1997) found that the EGRET data for W44 could result from bremsstrahlung and inverse Compton emission produced by a power-law distribution of relativistic electrons injected from a nearby pulsar with a spectral index of $\alpha = 1.66$, a value chosen to also self-consistently account for that remnant's hard radio spectrum. Chevalier (1999) and Bykov et al. (2000) fit the EGRET data of IC443 with bremsstrahlung emission produced by nonthermal electrons injected and accelerated in a inhomogeneous cloud environment. Good fits to the hard radio spectrum of IC443 ($\alpha \approx 0.36$) resulted from a high compression ratio (≈ 4.4) and, to a lesser extent, from the effects of second-order Fermi acceleration. Several authors have considered the emission of gamma-rays in SNR's resulting from the creation of neutral pions (and their subsequent decay) in collisions between shock-accelerated protons and the ambient gas (Sturmer et al. 1997; Gaisser et al. 1998; Baring et al. 1999). In these works, photons produced in the pionic cascade account for radiation emitted above ~ 100 MeV, and a population of accelerated (primary) electrons was invoked in order to produce bremsstrahlung emission to fill in the < 100 MeV portion of the EGRET spectrum. Sturmer et al. (1997) assume free-free absorption of the synchrotron emission by an intervening hot (8,000 K) ISM in order to produce a turnover at $\sim 10^7$ Hz which could then account for the seemingly hard spectrum of IC443. We note, however, that this warm component of the ISM has a filling factor of only ~ 0.2 , with most of the ISM, by volume, being filled by a hotter, lower density medium

(McKee & Ostriker 1977). Baring et al. (1999) showed that, in the presence of nonlinear shock acceleration, primary electrons could reproduce an unusually flat synchrotron radio spectrum that mimics that of IC443, but found that the resulting flux was well below the observed radio data. Clearly, the connection between the γ -ray and radio emissivities in these environments remains unsettled.

What has been lacking in previous works is a consistent treatment of the secondary leptons, themselves produced via proton-proton scatterings which, in addition to generating neutral pions, also produce charged pions. The latter decay into muons and thence into electrons and positrons. The vast array of multi-wavelength observations may now be brought to bear on the question of which of these populations—primary or secondary—dominate the radiative emission from these sources, requiring a more comprehensive and self-consistent treatment than has been attempted up until now.

An important caveat to the study of gamma-ray production in SNR's has been the identification of Sgr A East, a supernova-like remnant situated at the Galactic center, with the EGRET source 3EG J1746-2852 (Mayer-Hasselwander et al. 1998). Like several of the EGRET SNR's, Sgr A East has also been observed at 1720 MHz (the transition frequency of OH maser emission). Specifically, several maser spots have been resolved at the structure's SE boundary with velocities of ≈ 50 km s $^{-1}$, and an additional spot has been observed near the Northern arm of Sgr A West (a ~ 6 -pc mini-spiral structure of ionized gas orbiting about the center) at a velocity of 134 km s $^{-1}$ (Yusef-Zadeh et al. 1996). These observations indicate the presence of shocks at the interface between the expanding Sgr A East shell and the surrounding dense molecular cloud.

Interestingly, the energy required to carve out the radio synchrotron structure within the surrounding high density cloud during the creation of Sgr A East appears to have been extreme ($\sim 4 \times 10^{52}$ ergs; Mezger et al. 1989). An analogous viewpoint was adopted by Melia et al. (1998) in their analysis of Sgr A East's current high-energy radiative output, which also appears to be very high (by a factor of 50–100) compared to that of other SNR's. Recent observations made with the ACIS detector on board the *Chandra* X-ray Observatory, however, support the hypothesis that Sgr A East is more or less a typical single, mixed-morphology supernova remnant with an age of $\sim 10,000$ years (Maeda et al. 2003), casting some doubt on the interpretation of an unusually powerful explosion made earlier by Mezger et al. (1989).

A possible kinship between the EGRET SNR's and Sgr A East has more recently been explored by Fatuzzo & Melia (2003; hereafter FM03), who adopted the same mechanism—the decay of neutral pions created in proton-proton collisions—to account for the high-energy (> 100 MeV) emission in the Galactic center remnant. However, the work undertaken by

FM03 invoked two key elements generally ignored in earlier treatments of pion-decay scenarios. The first is a correct treatment of the energy-dependent pion multiplicity and its effect on the spectral shape of the pion-decay photons (Markoff et al. 1999; Melia et al. 1998). The second is the self-consistent use of secondary leptons (by-products of charged pion decay) in the determination of the broadband emission spectrum. The importance of these secondaries becomes evident with a proper treatment of the pion multiplicity, as each relativistic proton produces on average 40 - 60 leptons. As a result, the ratio of secondary leptons to shock-accelerated protons can be significantly higher than has previously been estimated using an assumed pion-multiplicity of three. This brings into question earlier work on pion-production mechanisms that ignored the role of these decay products. Indeed, the decay of charged pions into muons and, subsequently, into “secondary” relativistic electrons and positrons, results in a bremsstrahlung emissivity that contributes to the observed spectrum below ~ 100 MeV. And very importantly, secondary leptonic synchrotron emission also self-consistently accounts for the unusually steep ($\alpha \sim 1$) radio spectrum detected from Sgr A East’s periphery.

The purpose of this paper is to determine what role, if any, secondary leptons play in the EGRET SNR’s. As we shall see, secondary leptons alone cannot explain the broadband spectrum from these sources. Our results suggest that *both* primary electrons and secondary leptons must play an important role. We discuss the SNR-molecular cloud environment in §2. We then consider the role of secondary leptons produced in such an environment in §3, using the EGRET SNR IC443 as a case study. We show that while secondary leptons can account for the unusual radio spectrum of IC443, they alone cannot produce a pion-decay scenario that is fully consistent with the EGRET data. As such, we consider the role of primary electrons in IC443 in §4, and present a viable scenario in which both primary and secondary leptons contribute to the broadband emission of this SNR. In §5, we investigate whether this scenario can also account for the broadband observations of the EGRET SNR’s W44, W28, and γ -Cygni. We summarize our work and provide concluding remarks in §6.

2. The SNR-Cloud Environment

Molecular clouds contain a total mass of $\sim 10^5 M_{\odot}$ within a radius of ~ 20 pc, thereby having average densities of ~ 100 cm $^{-3}$. However, these regions of the interstellar medium are highly nonuniform, exhibiting hierarchical structure that can be characterized in terms of clumps and dense cores surrounded by an interclump gas of density $\sim 5 - 25$ cm $^{-3}$. Clumps have characteristic densities of $\sim 10^3$ cm $^{-3}$ and radii ranging from 0.1 – 1 pc. In all, these dense regions occupy a relatively small fraction (2 - 8 %) of the cloud volume, but

can account for most of its mass (e.g., Williams et al. 1995). More specifically, while a cloud may contain $\sim 10^3$ small ($\sim 1 M_\odot$) clumps, a significant fraction of the total cloud mass is located in a relatively small number (~ 20) of large, massive ($\sim 10^3 M_\odot$) clumps. These massive clumps, in turn, are comprised of $\sim 100 - 1000$ small (~ 0.1 pc), dense ($\sim 10^4 - 10^5$ cm $^{-3}$) cores (Lada et al. 1991; Jijina et al. 1999). While occupying a small total volume, these cores may contain as much as 19% of the cloud mass.

The observation of OH maser emission from SNR's that are interacting with molecular clouds has provided important clues about the SNR-cloud environment. High-resolution observations of W28, W44 and IC443 lead to the detection of 41, 25, and 6 individual maser spots, respectively, in each of these three remnants (Claussen et al. 1997). These spots appear to lie along, but displaced behind, the outer (leading) edge of the radio continuum emission. Since OH emission is associated with densities 10^4 cm $^{-3} < n < 5 \times 10^5$ cm $^{-3}$, these spots are presumably located within dense cores that have been overtaken by the expanding SNR shell.

The presence of maser emission has also provided valuable information about the magnetic fields in the SNR-cloud environments. In the simplest case, where flux freezing applies, the magnetic field strength in the interstellar medium scales as $B \propto \rho^{1/2}$. Indeed, an analysis of magnetic field strengths measured in molecular clouds yielded a relation between B and ρ of the form

$$B \sim 0.1 \text{ mG} \left(\frac{n}{10^4 \text{ cm}^{-3}} \right)^{0.47}, \quad (1)$$

although there is a significant amount of scatter in the data used to produce this fit (Crutcher 1999). This result is consistent with the idea that nonthermal linewidths, which are measured to be ~ 1 km s $^{-1}$ (e.g., Lada et al. 1991), arise from MHD fluctuations. The observed OH (1720 MHz) Zeeman splitting in the EGRET SNR's yields line of sight magnetic field strengths that range from 0.1 – 4 mG (Claussen et al. 1997; Koralesky et al. 1998; Brogan et al. 2000). While such field strengths can arise in the dense regions associated with the OH masers, these measurements may also point to an enhancement of the magnetic field, perhaps arising from shock compression. Indeed, Chevalier (1999) determined that the magnetic field strength in the SNR's radiative shell after compression is

$$B = 0.24 n_1^{1/2} v_2 \text{ mG}, \quad (2)$$

where n_1 is the interclump density in units of 10 cm $^{-3}$ and v_2 is the shock velocity in units of 100 km s $^{-1}$. Interestingly, Claussen et al. (1997) derived line-of-sight magnetic fields of order 0.2 mG over regions that were several parsecs apart in both W28 and W44. It should be noted, however, that the OH measured field strength may overestimate the fields by as much as a factor of 5 (Brogan et al. 2000).

Calculating the age of SNR’s expanding into a nonuniform medium is difficult, as can be witnessed by the large discrepancy in the ages determined for specific remnants. For example, estimates for the age of W44 range from 6000 - 7500 year (Rho et al. 1994) to $\sim 29,000$ years (Koo & Heiles 1995). Likewise, the age of IC443 has been estimated to be $\sim 1,000$ years (Wang et al. 1992), 3,000 year (Petre et al. 1988), and 30,000 years (Chevalier 1999). As elaborated upon below, a scenario whereby secondary leptons contribute significantly to the broadband emission of the EGRET SNR’s favors an age of 30,000 years. We therefore adopt this age throughout the rest of the paper.

3. The Role of Secondary Leptons in IC443

We demonstrate in this section that while a pion-decay mechanism with only secondary leptons can account for the high-energy spectrum of Sgr A East, a similar mechanism apparently cannot do so for the EGRET SNR’s. More specifically, while the high-energy (> 100 MeV) portion of the latter’s spectrum can be fit by the decay of neutral pions produced by collisions between power-law, shock-accelerated protons and the ambient medium, secondary leptons produced concomitantly via the decay of charged pions cannot reproduce the observed < 100 MeV emission. However, secondary leptons can account for the unusually hard radio spectra of the EGRET SNR’s.

There are two aspects of the secondary lepton distribution that make it incapable of accounting for the < 100 MeV emission in the EGRET SNR’s. First, the maximum power radiated by leptons is not expected to greatly exceed the luminosity generated via the decay of neutral pions, since the charged pion production rate mirrors (within a factor two) that of the neutrals. Second, leptons are injected into the system with a distribution that peaks near 50 MeV (see Figure 2 of FM03). Since cooling via electronic excitation dominates over bremsstrahlung for energies below ~ 100 MeV, a cooled distribution of secondaries will itself have a break near ~ 100 MeV. In turn, the high-energy emission of secondaries, which in the SNR environment is dominated by bremsstrahlung, steepens near 100 MeV. All these factors together preclude any possibility of the secondary leptons alone accounting for the whole EGRET SNR spectrum.

To clearly illustrate this point, we apply the model developed for Sgr A East to the γ -ray data pertaining to SNR IC443. Since the model is discussed extensively in FM03, we will not reproduce the details here. However, we note that for this study, we assume that the medium is comprised of neutral H, and hence adopt the appropriate bremsstrahlung and electronic excitation cooling rates given in Gould (1975). In addition, we use the atomic bremsstrahlung cross-section of Blumenthal & Gould (1970) to calculate the bremsstrahlung

emission. We note, however, that the choice of a neutral medium over a fully ionized one has little effect on our results.

The high-energy portion of the spectrum is fit quite well with the pion bump resulting from shock-accelerated protons characterized by a power-law distribution $dn_p/dE \propto E^{-\alpha_p}$ with a spectral index $\alpha_p = 2.2$ (that falls within the expected range of 2 - 2.4). However, the non-detection of the EGRET SNR's by Whipple (Buckley et al. 1998) and CANGAROO (Rowell et al. 2000) mandates a maximum energy E_{max} for this distribution. The spectrum is normalized by the product $n_H \cdot n_p \cdot V$, chosen on the basis of an assumed source distance of 1.5 kpc. Here, n_H is the proton number density in the ambient medium, n_p is the number density of shock-accelerated protons, and V is the volume of the emitting region.

For any given SNR, the number of secondary leptons depends on the injection rate, the rate at which these particles either lose energy or leave the system, and the duration over which particles have been injected in the system. Their γ -ray emissivity, primarily bremsstrahlung, peaks when they reach a steady state. The maximum bremsstrahlung emissivity below 100 MeV is correlated directly with the radiative flux produced by decaying neutral pions because both are ultimately produced by the same proton-proton scattering events. (Note, however, that secondary leptons that produce higher energy emission can cool more efficiently via synchrotron emission, in which case the above claim cannot be made.)

This result holds regardless of the number density n_H of the ambient medium, because the density of steady-state secondary leptons that emit via bremsstrahlung scales inversely with n_H . This dependence offsets the $\propto n_H$ variation of the emissivity. Of course, the bremsstrahlung spectrum also depends upon the choice of magnetic field strength, but only at sufficiently high-energies (typically $> 10^3$ MeV) so that synchrotron cooling dominates over bremsstrahlung. The resulting spectral shape below 10^3 MeV is therefore completely specified by the single parameter α_p , and is fit to the data through the single choice of the product $n_H \cdot n_p \cdot V$. This “universal” curve is shown by the solid line in Figure 1 for $\alpha_p = 2.2$ (and $E_{max} = 10^6$ MeV), together with the EGRET data and Whipple upper-limit pertaining to SNR IC443. Clearly the bremsstrahlung emission due to secondary leptons alone cannot account for the spectrum below 100 MeV—a result that also holds (and is even more pronounced) for W28, W44, and γ -Cygini.

Compounding the secondary lepton's inability to produce the bremsstrahlung emission required to “fill in” the sub-100 MeV portion of the EGRET spectrum is the fact that a steady-state assumption is difficult to justify in the SNR environment. This point is illustrated by Figure 2, which shows the lepton cooling time (defined as $\tau_{cool} = E/\dot{E}$) as a function of lepton energy associated with bremsstrahlung (short dashed), synchrotron (long dashed), inverse Compton scattering with the Cosmic Microwave Background (dotted) and

electronic excitation (solid) for a neutral medium with a density of $n = 300 \text{ cm}^{-3}$ and field strength of $B = 0.3 \text{ mG}$. It is clear that even for the assumed remnant age of 30,000 years, the steady-state assumption would require densities in excess of $\sim 1000 \text{ cm}^{-3}$. Such densities are well above the average cloud density and the expected density of the radiative shell ($\sim 500 \text{ cm}^{-3}$; see Chevalier 1999). It does not appear, therefore, that leptons have sufficient time to reach steady state. To illustrate this point further, we plot in Figure 3 the steady-state lepton distributions arising from the production of the pion-bump shown in Figure 1 for two values of n_H : 300 cm^{-3} and $3,000 \text{ cm}^{-3}$. Since the lepton injection rate is fixed by the normalization of the pion bump to the EGRET data (and therefore independent of the ambient density), the steady-state distribution for the $n_H = 300 \text{ cm}^{-3}$ case (dotted line) attains a higher value than its high-density counterpart (dashed line). The solid line represents the lepton distribution attained by simply multiplying the injection rate by an age of 30,000 years. As can be seen, the built-up injected distribution falls below the lower-density steady-state distribution over most of the energy range. As such, a more realistic secondary lepton emissivity is represented by the dotted line in Figure 1, which shows the bremsstrahlung emission produced by the secondary leptons associated with the lower-density case. For simplicity, we have assumed that the true particle distribution for the lower-density (non steady-state) case is given by the lower of the solid and dashed curves in Figure 3, and adopt such a convention throughout this paper.

An underlying assumption made in the above discussion of the lepton distribution is that the injection rate is constant in time. In turn, this assumes that the proton distribution and the ambient medium with which it interacts do not change over the remnant's evolution. One could speculate an earlier brief period of significantly higher injection, so that the lepton distribution assumed above significantly underestimates the true lepton population. However, such an epoch would imply that a considerably larger number of relativistic protons permeated the region during this highly active era ($\sim 10^2$ greater than is presently inferred). Such a scenario is therefore energetically unfavorable. Specifically, for a distance of 1.5 kpc to IC443, the energy content in relativistic protons that produce the pion-bump shown in Figure 1 is

$$E \approx 0.004 \times 10^{51} \text{ ergs} \left(\frac{n_H}{300 \text{ cm}^{-3}} \right)^{-1}. \quad (3)$$

A significantly larger proton population would thus seem energetically untenable. In addition, one would also need to argue that protons have diffused out of the SNR environment, whereas the leptons did not.

While secondary leptons do not appear capable of accounting for the observed gamma-ray emissivity, they do appear to be capable of accounting for the unusually hard radio spectra observed from the EGRET SNR's. To explore this issue, we consider the synchrotron

emissivity of secondary leptons produced under a baseline set of parameters $\alpha_p = 2$, $E_{max} = 10^6$ MeV, $B = 0.29$ mG, and $n_H = 300$ cm $^{-3}$ (case A). We sample the parameter space around our baseline point by considering the following additional cases: B) same as A but with $E_{max} = 10^5$ MeV; C) same as A but with $\alpha_p = 2.4$; D) same as A but with $n_H = 3000$ cm $^{-3}$ and $B = 0.45$ mG. All cases have an assumed age of 30,000 year, and are normalized to the EGRET data as shown in Figure 4. The resulting synchrotron emissivity for these cases is then shown in Figure 5, where the radio data for IC443 were taken from Erickson & Mahoney (1985). Solid circles refer to data that were corrected via a calibration factor, whereas open circles refer to data for which such a correction was not possible. The effect of free-free absorption by the warm component of the ISM is not included in the radio fits. Since this component has an expected electron density of $n_{ew} = 0.17$ cm $^{-3}$ and a temperature of $T = 8000$ K (McKee & Ostriker 1975), the resulting absorption coefficient is $\alpha_{ff} \approx 6 \times 10^{-23}$ at a frequency of $\nu = 10^7$ Hz (see, e.g., Sturner et al. 1997). For a source distance of 1.5 kpc and a filling factor of ~ 0.2 , free-free absorption is unlikely to have a significant effect on the radio spectra of IC443 above $\sim 10^7$ Hz, although it may be responsible for the apparent low-energy turnover at around that frequency as suggested by the data presented in Figure 5 (see also Figure 14).

There are several important constraints that the radio data place on the pion-decay scenario. Specifically, if the radio emission does indeed arise from secondary leptons, then such an association would favor a proton distribution with a spectral index of 2 and a high-energy cut-off of $\sim 10^6$ MeV. In addition, this association clearly favors a lower-density ($< 10^3$ cm $^{-3}$) environment and a remnant age of $\sim 30,000$ year. Although a younger age can be adopted, doing so would lower the number of secondary leptons, and hence, would require a stronger magnetic field to compensate. Adopting a younger age would then be in conflict with the measured fields in the EGRET SNR's of ~ 0.2 mG (see §2). We note that for densities below 10^3 cm $^{-3}$, the lepton distribution over the energy range responsible for the observed radio emission is independent of the ambient density since it is just the injected distribution built up over the age of the remnant. Once one reaches sufficiently high densities, the lepton distribution is then set by its steady-state value, and scales as the inverse of n_H (see Figure 3). As a result, the magnetic field required for case D is greater than those of cases A - C.

It is quite intriguing that the radio data are fit so well by case A since such densities and field strengths are expected in the radiative shells of SNR's interacting with molecular clouds (Chevalier 1999). In addition, a 0.29 mG magnetic field is consistent with observations (see §2 above).

We conclude from the analysis presented in this section that secondary leptons produced

in a pion-decay scenario cannot account for the sub-100 MeV γ -ray emission required to make such a scenario compatible with the EGRET data over all energies. However, this population of leptons can seemingly account for the unusually hard radio spectra observed from the EGRET SNR's. Although the focus of our discussion thus far has been on IC443, our conclusions also hold for W28, W44 and γ -Cygni (as further discussed in §5).

4. The Role of Primary Electrons in the Nonhomogeneous Medium of IC443

The fact that secondary leptons cannot reproduce the γ -ray spectrum of the EGRET SNR's below 100 MeV suggests the presence of an additional electron population in these sources. Yet the radio data are explained rather well by the former, so the physical conditions where these other particles operate are severely constrained in terms of their synchrotron emissivity. At best, a combination of primary and secondary leptons may be responsible for the radio emission.

Let us adopt the view that the diffusive shock mechanism responsible for accelerating the protons also energizes a power-law distribution of (“primary”) electrons. From previous works (e.g., Gaisser et al. 1998), it is known that the EGRET data from IC443 can be reproduced by a scenario in which both the primary electrons and protons have a spectral index of $\alpha = 2.4$. However, the resulting secondary leptons would then be too steep to provide a good fit to the radio data (see Case C in Figure 5). Furthermore, it is not difficult to see that the γ -ray spectra of the EGRET SNR's are actually compliant to an even steeper primary electron distribution. We therefore consider the possibility that the primary electron population is injected with a power-law distribution $\propto E^{-\alpha_e}$ whose spectral index α_e is different from α_p .

In Figure 6 we show fits to the γ -ray spectrum of IC443 for our pion-decay scenario with a proton spectral index of $\alpha_p = 2$ and cutoff energy of 10^6 MeV, and an ambient medium of density $n_H = 300 \text{ cm}^{-3}$ and field strength $B = 0.29 \text{ mG}$ (case A above), but with the addition of bremsstrahlung emission from a power-law distribution of primary electrons in equipartition with the proton distribution, and normalized to the sub-100 MeV EGRET data. The latter constraints lead to a value of $\alpha_e = 2.8$. Such a steep electron distribution almost certainly implies nonlinearity in the shock. While the primary electron distribution index α_e is not well constrained, it is not clear whether α_p and α_e can differ by so much. Still, values of α_e this large have emerged from both analytical and (highly detailed) numerical simulations of particle acceleration in certain energy ranges, so they cannot be ruled out easily (see, e.g., Baring et al. 1999; Ellison et al. 2000).

While the assumed population of primary leptons can provide the necessary bremsstrahlung emission to produce a good fit to the EGRET data, as shown in Figure 6, it is not compatible with the radio data if located in the same region as the secondary leptons. This point is illustrated in Figure 7, which shows the synchrotron emissivities of the secondary leptons (dashed curve) and the primary electrons (solid curve) for a common field strength of 0.29 mG. This result suggests that the inhomogeneity of the SNR-cloud environment results in two distinct emission zones for the primary and secondary populations.

Taking our cue from the observation of OH masers (see §2), we consider the possibility that particle acceleration (both proton and electron) occurs as dense cores are overtaken by the expanding radiative shell. Interestingly, it takes $\sim 10^3$ years for a shell moving at ~ 100 km s $^{-1}$ to sweep past a 0.1 pc core. With the radiative shell expanding several parsecs into the cloud, an appreciable fraction of the roughly 10^4 cores would have been overtaken, and thus, have been active acceleration sites. An active epoch lasting $\sim 10^2 - 10^3$ years in a given core could thus be consistent with the number of observed maser spots in W44, W28, and IC443 (see §2). Indeed, these observations would suggest that roughly 500 to 5,000 cores have been activated in each of these regions.

In these high-density environments ($\sim 5 \times 10^4$ cm $^{-3}$), the accelerated electrons would cool in ~ 300 years. If the time for particles to diffuse out of these dense regions was appreciably longer than the cooling time (but shorter than the age of the remnant), then the electrons would efficiently radiate most of their power while still in these regions. On the other hand, the protons in these cores have a cooling time of order $\sim 10^3$ years and could therefore diffuse into the lower density radiative shell before losing an appreciable amount of energy. In order to explore this scenario, we consider the injection of electrons and protons into cores with density of 5×10^4 cm $^{-3}$ and field strength $B = 0.22$ mG (from Eq. 1). We assume that the protons diffuse into the lower density radiative shell, thus reproducing the scenario explored in case A above. In contrast, the electrons are assumed to radiate most of their power in the dense regions before diffusing out. We approximate the resulting bremsstrahlung emission by calculating the steady-state distribution produced by the injection of power-law electrons with $\alpha_e = 2.8$ in equipartition with the proton distribution, but confined to the high-density cores. The resulting γ -ray emissivities are presented in Figure 8, with the short and long dashed curves as in Figure 6, and the dotted curve representing the ensuing primary electron bremsstrahlung emissivity. Because electronic excitation effectively cools the electrons below 100 MeV, the steady-state distribution is less steep in the lower-energy range and, as a result, produces a bremsstrahlung emissivity that does not fit the lowest energy data point.

Given the nature of nonlinear shocks, it may be possible that the electron distribution

steepens significantly at energies > 10 MeV, thereby providing a good fit to the EGRET data without violating the imposed equipartition constraint. Indeed, the resulting γ -ray emissivity (calculated in the same manner as for Figure 8) for an electron distribution with $\alpha_e = 3.4$ is shown in Figure 9, demonstrating the viability of this scenario in accounting for the observed spectrum of IC443. The radio spectrum of the primary electrons is approximated by assuming that the steady-state distribution derived in the high-density medium also describes the electrons after they have diffused into the radiative shell. The resulting synchrotron emissivity for the primary electrons (dashed curve), along with the emissivity of the secondary leptons (solid curve), is shown in Figure 10. Clearly, the primary electrons cool effectively in the high-density environment before diffusing out into the shell, so that their synchrotron emissivity falls well below that of the secondaries.

The total energy content of the proton distribution required to fit the EGRET data is given by Equation 3, and therefore represents a small fraction of the overall blast energy. However, the acceleration of particles at numerous localized sites places stronger constraints on the model energetics. For example, with an assumed activation of ~ 5000 cores, each with radius ~ 0.1 pc, the total cross-sectional area of “active sites” energized by the expanding shell is roughly 0.06% of the total shell’s surface area (for an assumed shell radius of 15 pc). Clearly, this scenario thus requires a very high particle acceleration efficiency at the shell-core interface.

5. The Two-Zone Emission Model: Application to W28, W44 and γ -Cygni

In the previous section, we presented a two-zone emission model to self-consistently account for both the γ -ray and radio data observed from IC443. In this section, we apply this model to W28, W44, and γ -Cygni. Although there are several free parameters that can be varied, we set the proton distribution high-energy cut-off, the primary electron spectral index, the shell density, the core density, and the remnant age to values of $E_{max} = 10^6$ MeV, $\alpha_e = 3.4$, $n_H = 300$ cm $^{-3}$, $n_{Hc} = 5 \times 10^4$ cm $^{-3}$, and 30,000 year, respectively. We treat α_p and B as free parameters, and normalize the proton and primary electron distributions through fits to the EGRET data.

The results for W44 are shown in Figures 11 - 12, where the free parameters are $\alpha_p = 2.0$ and $B = .43$ mG. The results for W28 are shown in Figures 13 - 14, where the free parameters are identical to those chosen for W44. The results of γ -Cygni are shown in Figures 15 - 16, where $\alpha_p = 2.2$ and $B = .28$ mG. In all, the two-zone model presented here provides good fits to the radio and γ -ray data observed from the EGRET SNR’s.

6. Conclusions

An earlier analysis of the high-energy emission from Sgr A East has shown that its radio and γ -ray spectra may be understood self-consistently in the context of neutral pion production in proton-proton scatterings and their subsequent decay into photons and relativistic (secondary) leptons. The latter, in particular, account for this remnant’s radio emission with the correct spectral shape and flux, once the ambient physical conditions are understood from fits to the γ -ray data.

A similar analysis of the other EGRET SNR’s has now revealed that secondary leptons may account for most (if not all) of the SNR radio spectrum. Interestingly, the environment required to produce good fits to the radio data are consistent with those expected from a dense ($n_H \sim 500 \text{ cm}^{-3}$) and highly-magnetized ($B \sim 0.3 \text{ mG}$) shell, and is consistent with the observed magnetic field strengths inferred from these regions. However, a pion decay scenario with only secondary leptons cannot account for the observed γ -ray spectra. It therefore appears that a population of shock-accelerated electrons must also be present.

Given the constraints imposed on the primary electrons by the radio data, and taking our cue from the observation of several OH maser spots observed in the SNR environments, we have presented a two-zone model wherein protons and electrons are accelerated in the dense cores of molecular clouds that are energized by the expanding SNR shell. While as many as $\sim 5,000$ such cores may have been energized in these environments, a relatively short “active” era (lasting $\sim 10^2 - 10^3$ years) could then explain the observed number of OH maser spots. In addition, if the electron cooling time in these dense regions (~ 300 years) is shorter than the diffusion time, these electrons would cool effectively within the cores before diffusing out into the radiative shell. Their resulting synchrotron emissivity would then fall below the observation limits. In contrast, the longer cooling time for the protons could allow them to diffuse out into the shell before producing pions via $p-p$ collisions with the ambient medium.

We find that the two-zone model provides good fits to the radio and γ -ray data for IC443, W44, W28 and γ -Cygni so long as the primary electrons are injected with a steep $\alpha_e = 3.4$ power-law distribution above 10 MeV (in order to not violate the imposed condition that this distribution be injected with the same energy as the proton distribution.) Such a distribution would then signal the importance of nonlinear effects in shock acceleration. In addition, our model suggests that the EGRET SNR’s are $\sim 30,000$ years old. While at the high end of the inferred ages for these remnants, this result may help explain why most of the SNR’s that also produce OH maser emission (and are therefore interacting with dense regions of molecular clouds) have not been observed in γ -rays, as they may not be old enough to have built up populations of relativistic particles capable of producing an

observable emissivity. Finally, while the total energy in relativistic particles represents a small (< 1%) fraction of the total blast energy, the association of acceleration sites with dense cores suggests that a large percentage of the local energy ($\sim 10\%$) must be converted into nonthermal particle energy.

An outstanding issue raised by this work is whether the two-zone model invoked to account for the broadband emission of the EGRET SNR's is consistent with the picture developed by FM03 for Sgr A East. In the work of FM03, particle diffusion out of the Sgr A East environment was required to produce the steep lepton distribution inferred from the radio data. Such a diffusion process was not required in this work. However, recent observations of the Galactic center by HESS (Aharonian et al. 2004) suggest that there may be two acceleration regions in Sgr A East (Crocker et al. 2004), thereby complicating the overall picture. In addition, the possible association of the AGASA and SUGAR anisotropies at energies $\sim 10^{18}$ eV near the Galactic center with particle acceleration at Sgr A East (Crocker et al. 2004) casts some doubt on the diffusion scenario invoked by FM03. In light of this work and recent observations, a detailed re-examination of the pion-decay model in Sgr A East is therefore warranted.

Acknowledgments

We are grateful to Matthew Baring and Fred Adams for very helpful discussions. This research was supported in part by NASA grant NAG5-9205 and NSF grant AST-0402502 at the University of Arizona. MF is supported by the Hauck Foundation through Xavier University.

REFERENCES

Aharnian, F. A. et al. 2004, pre-print (astro-ph/0408145). Submitted to AA.

Baring, M. G., et al. 1999, ApJ, 513, 311

Blumenthal, G. R., & Gould, R. J. 1970, Reviews of Modern Physics, 42, 237

Brogan, C. L., Frail, D. A., Goss, W. M., & Troland, T. H. 2000, ApJ, 537, 875

Buckley, J. H. et al., 1998, AA, 329, 639

Bykov, A. M., Chevalier, R. A., Ellison, D. C., & Uvarov, Yu. A. 2000, ApJ, 538, 203

Chevalier, R. A. 1999, ApJ, 511, 798

Claussen, M. J., Frail, D. A., Goss, W. M., & Gaume, R. A. 1997, ApJ, 489, 143

Crocker, R. M., Fatuzzo, M., Jokipii, R., Melia, F., & Volkas, R. R. 2004, pre-print (astro-ph/0408183). Accepted for publication to ApJ.

Combi, J. A., Romero, G. E., & Benaglia, P. 1998, A&A, 331, L91

Combi, J. A., et al. 2001, A&A, 366, 1047

Crutcher, R. M. 1999, ApJ, 520, 706

de Jager, O. C., & Mastichiadis, A. 1997, ApJ, 482, 874

Ellison, D.C., Berezhko, E.G., and Baring, M.G., 2000, ApJ, 540, 292

Erickson, W. C. and Mahoney, M. M., 1985, ApJ, 290, 596

Esposito, J. A., Hunter, S. D., Kanback, G., & Streekumar, P. 1996, ApJ, 461, 820

Fatuzzo, M., & Melia, F. 2003, ApJ, 596, 1035 (FM03)

Gaisser, T. K., Protheroe, R. J., & Stanev, T. 1998, ApJ, 492, 227

Gould, R. J. 1975, ApJ, 196, 689

Jijina, J., Myers, P. C., & Adams, F. C. 1999, ApJS, 125, 161

Kassim, N. 1989, ApJS, 71, 799

Koo, B.-C., & Heiles, C. 1995, ApJ, 442, 679

Koralesky, B., Frail, D. A., Goss, W. M., Claussen, M. J., & Green, A. J. 1998, *ApJ*, 116, 1331

Lada, E. A., Bally, J., & Stark, A. A. 1991, *ApJ*, 368, 432

Maeda, Y., et al. 2002, *ApJ*, 570, 671

Markoff, S., Melia, F., & Sarcevic, I. 1999, *ApJ*, 522, 870

Mayer-Hasselwander, H. A., et al. 1998, *A&A*, 335, 161

McKee, C. F., & Ostriker, J. P. 1977, *ApJ*, 218, 148

Melia, F., Fatuzzo, M., Yusef-Zadeh, F., & Markoff, S. 1998, *ApJ*, 508, L65

Mezger, P., et al. 1989, *A&A*, 209, 337

Pedlar, A., et al. 1989, *ApJ*, 342, 769

Petre, R., Szymkowiak, A. E., Seward, F. D., & Willingale, R. 1988, *ApJ*, 335, 215

Rho, J.-H., Petre, R., Schlegel, E. M., & Hester, J. J. 1994, *ApJ*, 430, 757

Rowell, G.P. et al. 2000, *AA*, 359, 337

Sturner, S. J., Skibo, J. G., Dermer, C. D., & Mattox, J. R. 1997, *ApJ*, 490, 619

Wang, Z. R., Asaoka, I., Hayakawa, S., & Koyama, K. 1992, *PASJ*, 44, 303

Williams, J. P., Blitz, L., & Stark, A. A. 1995, *ApJ*, 451, 252

Yusef-Zadeh, F., Roberts, D. A., Goss, W. M., Frail, D. A., & Green, A. J. 1996, *ApJ*, 466, L25

Yusef-Zadeh, F., Roberts, D. A., Goss, W. M., Frail, D. A., & Green, A. J., 1999, *ApJ*, 527, 172

Yusef-Zadeh, F., Wardle, M., Rho, J., & Sakano, M. 2003, *ApJ*, 585, 319

Zhang, X., Zheng, Y., Landecker, T. L., and Higgs, L. A., 1997, *AA*, 324, 641

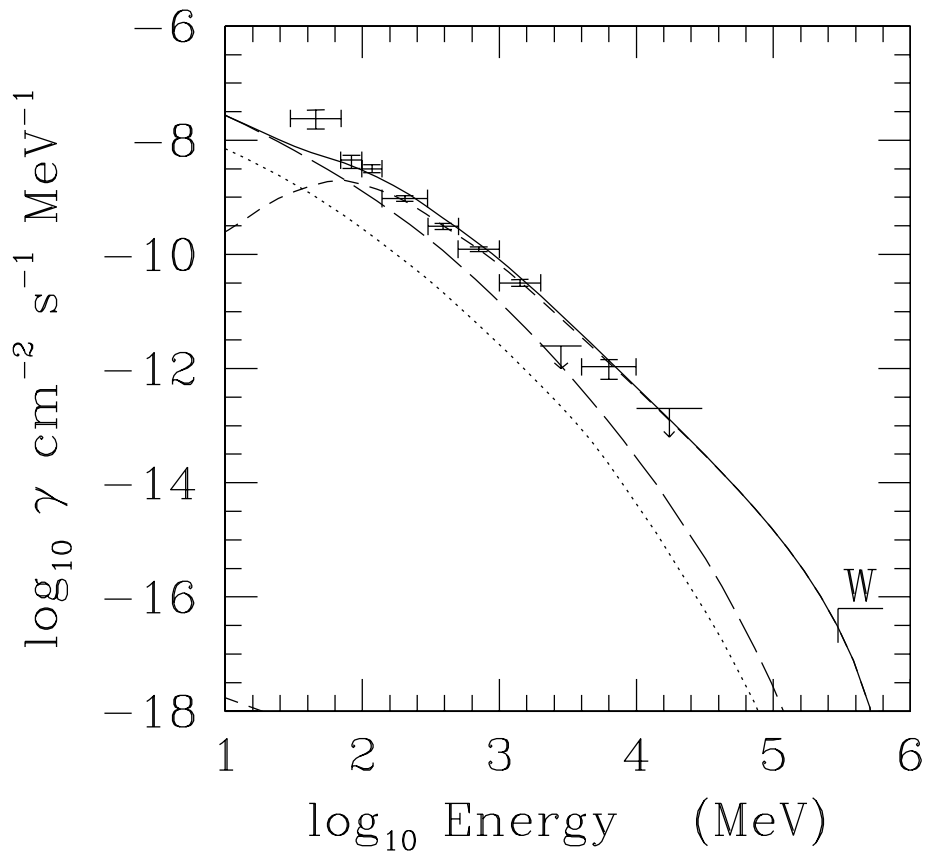


Fig. 1.— Secondary lepton model for IC443 for a proton distribution with a spectral index of $\alpha_p = 2.2$ and a high-energy cutoff of $E_{max} = 10^6$ MeV. Short dashed curve: photons produced via neutral pion decay from proton-proton scattering events; long dashed curve: bremsstrahlung emission from the secondary leptons produced via charged pion decays for a steady-state distribution; solid curve: total spectrum for the steady state scenario; dotted curve: bremsstrahlung emission from the secondary leptons for an ambient density of $n_H = 300$ cm $^{-3}$ and an injection duration of 30,000 years. Data are taken from Esposito et al. (1996) and Buckley et al. 1998.

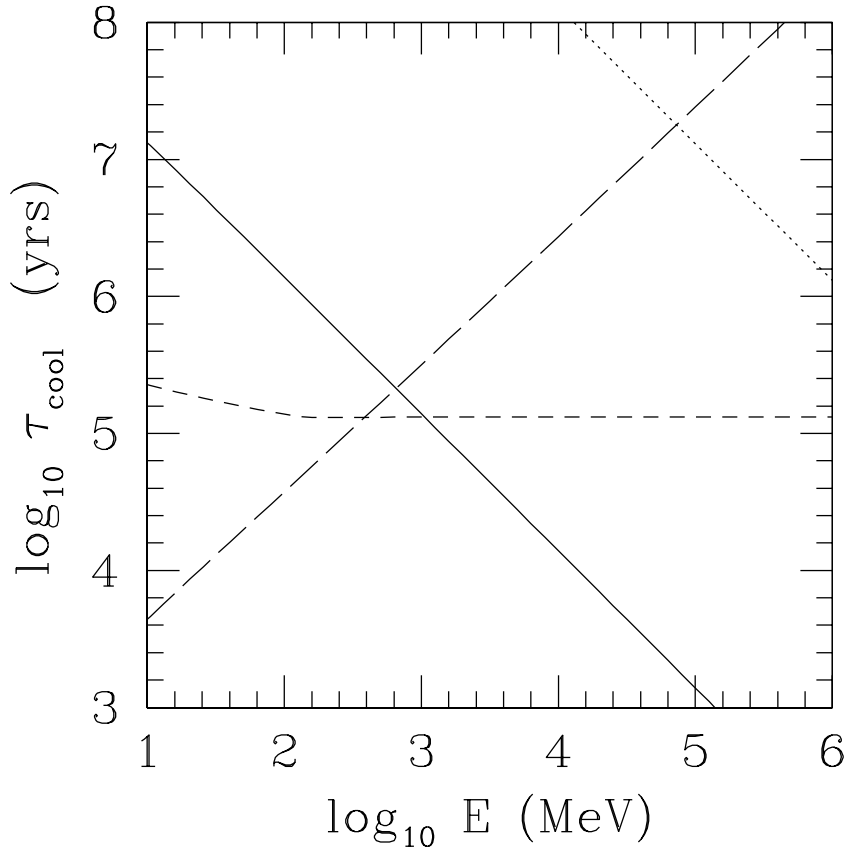


Fig. 2.— The cooling time $\tau_{cool} = E/\dot{E}$ as a function of energy for leptons interacting with a neutral medium of density $n_H = 300 \text{ cm}^{-3}$ and magnetic field strength $B = 0.3 \text{ mG}$. Short dashed curve: bremsstrahlung cooling; long dashed curve: synchrotron cooling; solid curve: electronic excitation losses; dotted curve: inverse Compton scattering with the Cosmic Microwave Background.

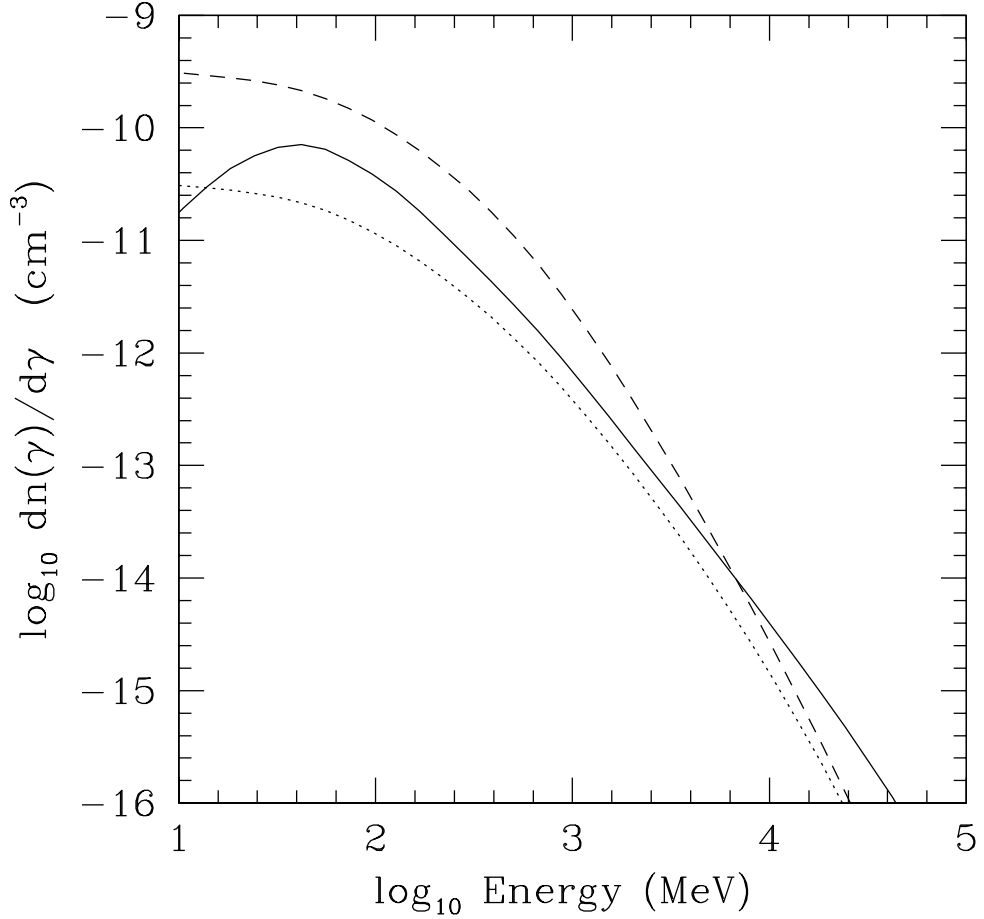


Fig. 3.— Steady-state lepton distributions arising from the pion-decay mechanism used to fit the pion-bump shown in Figure 1. The dotted line depicts the ensuing steady-state distribution for an assumed ambient density of $n_H = 3,000$ cm $^{-3}$, whereas the dashed curve shows the steady-state distribution for a density of $n_H = 300$ cm $^{-3}$. The solid line represents the lepton injection rate (which is tied to the EGRET data, and therefore independent of n_H) multiplied by the assumed age of 30,000 years.

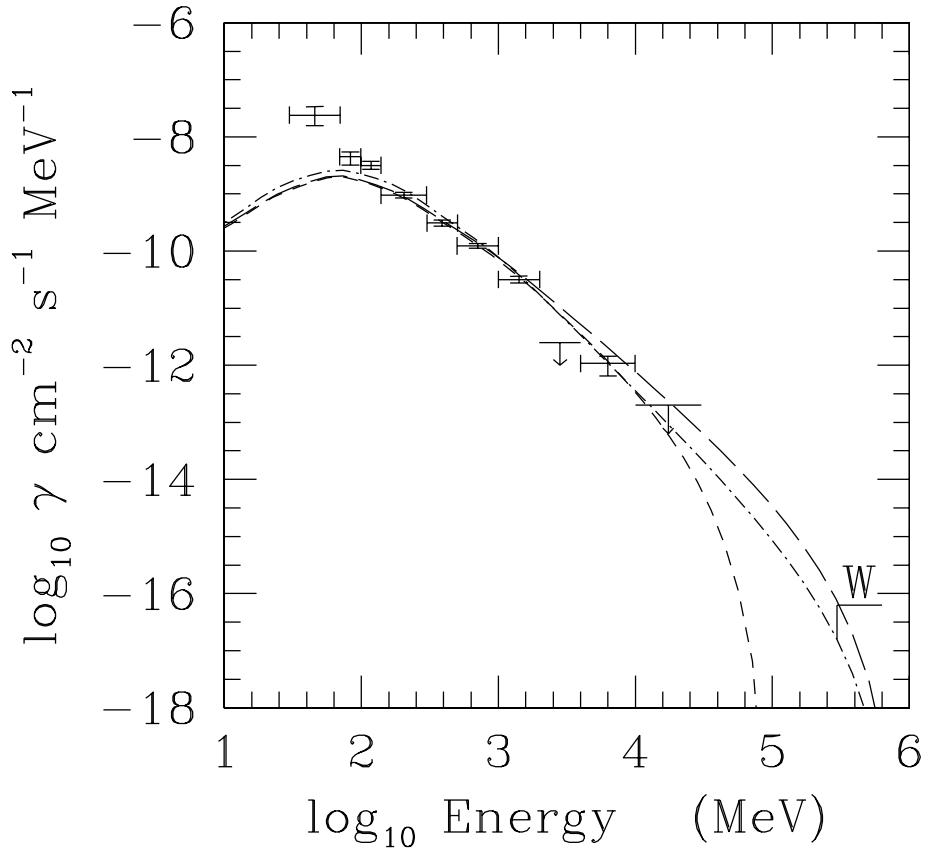


Fig. 4.— Photons produced via neutral pion decay arising from the interaction between a relativistic power-law distribution of protons with spectral index α_p and high-energy cutoff E_{max} , and an ambient medium of density n_H and field strength B . Fits are normalized to IC443. Long dashed curve – case A: $\alpha_p = 2.0$, $E_{max} = 10^6$ MeV, $n_H = 300$ cm $^{-3}$, $B = 0.29$ G; short dashed curve – case B: same as Case A but with $E_{max} = 10^5$ MeV; dot-dashed curve – case C: same as Case A but with $\alpha_p = 2.4$; Case D (same as case A but with $n_H = 3,000$ cm $^{-3}$ and $B = 0.45$ mG) produces the same curve as case A, and is therefore also represented by the long dashed curve.

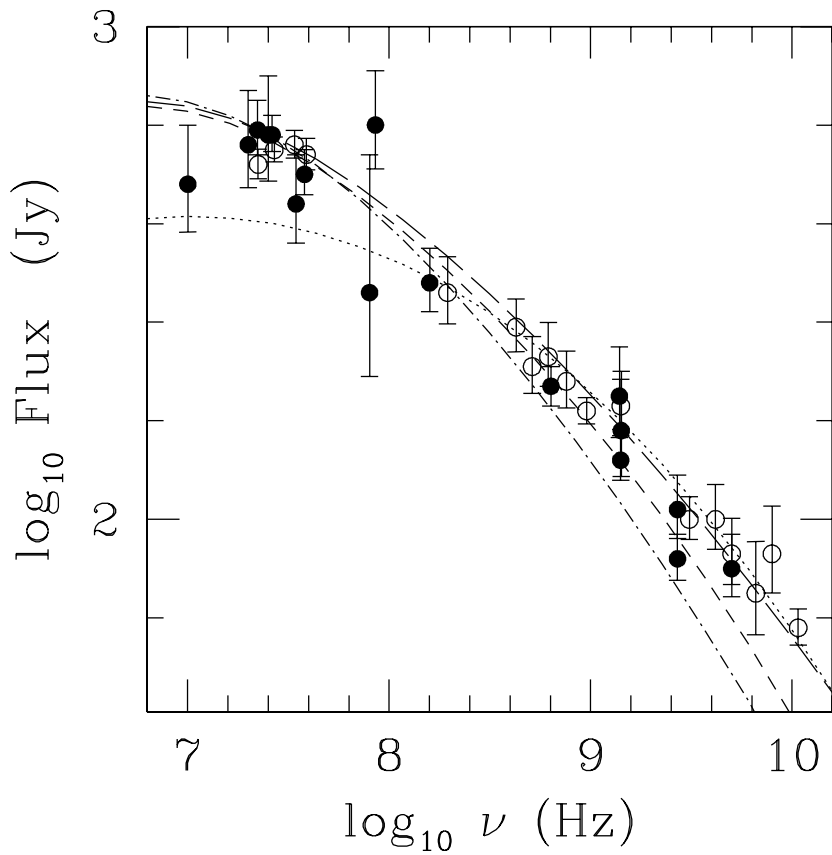


Fig. 5.— Radio synchrotron emission produced by secondary leptons associated with the four cases presented in Figure 4. Long dashed curve: case A; short dashed curve: case B; dot-dashed curve: case C; dotted curve: case D. Radio data for IC443 taken from Erickson & Mahoney 1985.

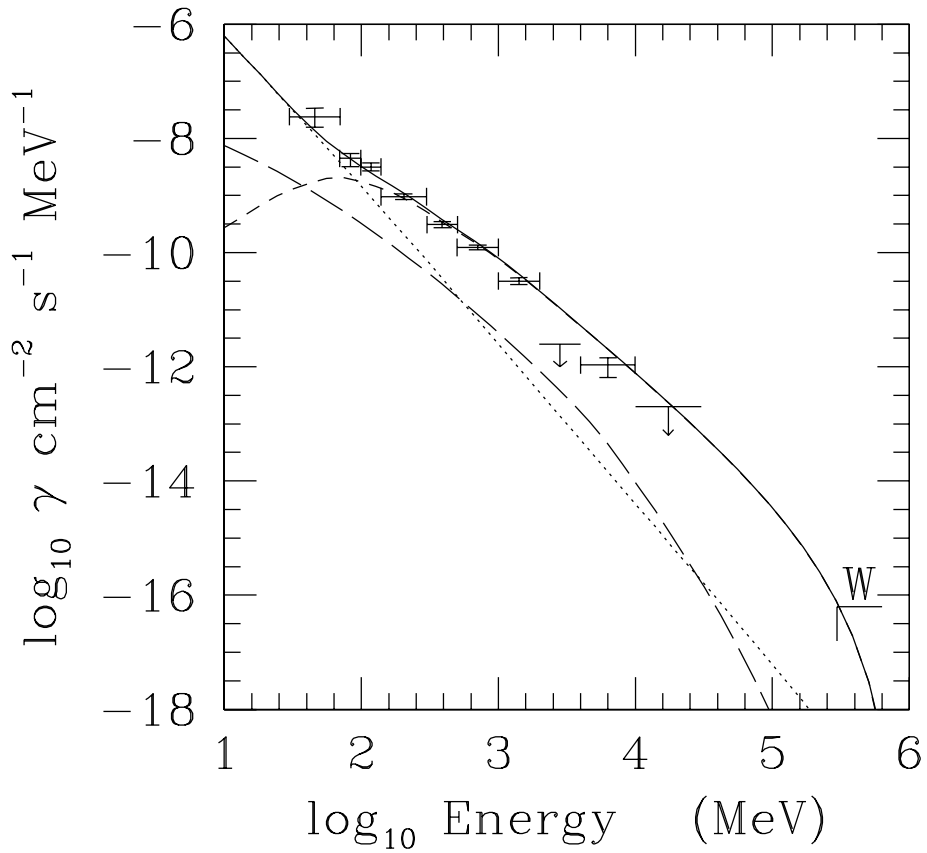


Fig. 6.— The γ -ray emissivity from our pion-decay model with $\alpha_p = 2$, $E_{max} = 10^6$ MeV, $n_H = 300 \text{ cm}^{-3}$ and $B = 0.29 \text{ mG}$ and as assumed primary electron population with spectral index of $\alpha_e = 2.8$. The remnant's age is assumed to be 30,000 years in order to determine the secondary leptons' (non steady-state) distribution. Short-dashed line: photons produced via the decay of neutral pions; long dashed curve: bremsstrahlung emission from the secondary leptons; dotted line: bremsstrahlung emission from the primary electron population.

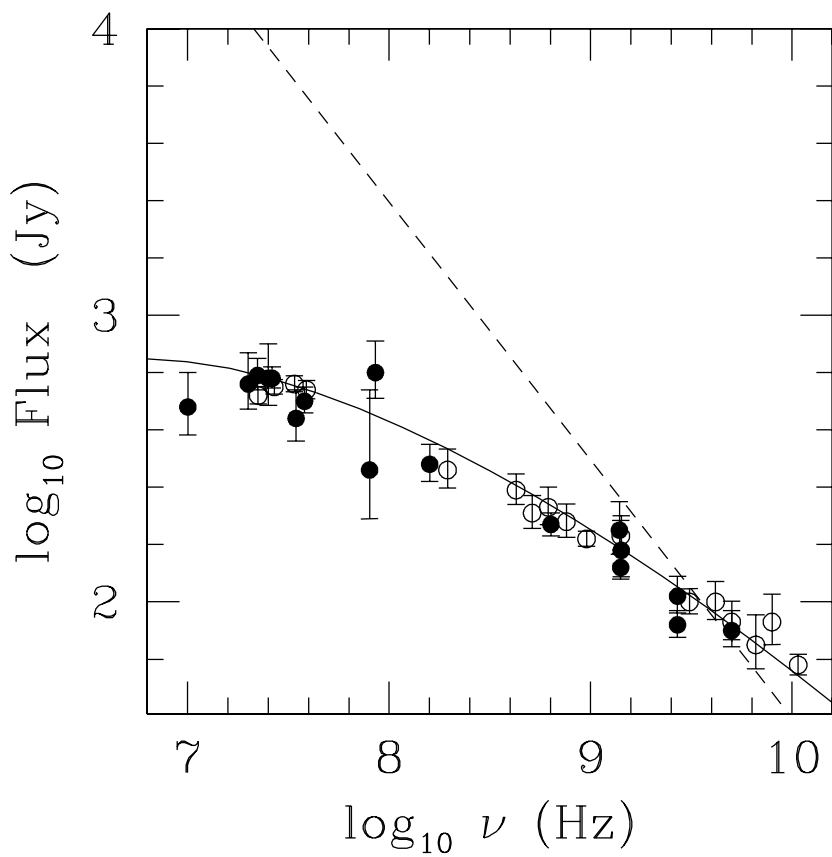


Fig. 7.— The synchrotron emission produced by the primary electrons (dashed curve) and secondary leptons (solid curve) associated with the curves presented in Figure 6 for a field strength of $B = 0.29$ mG.

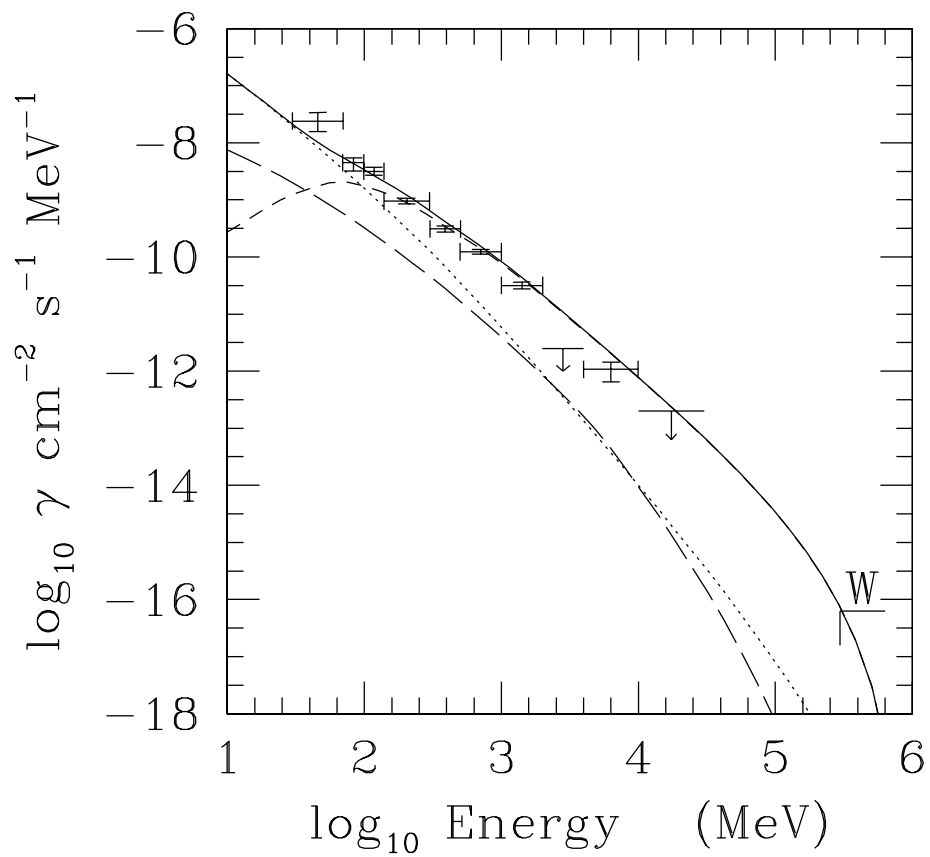


Fig. 8.— Same as Figure 6, but for a steady-state population of primary electrons injected into the dense core environment with a spectral index of $\alpha_e = 2.8$ at the same energy rate as the protons.

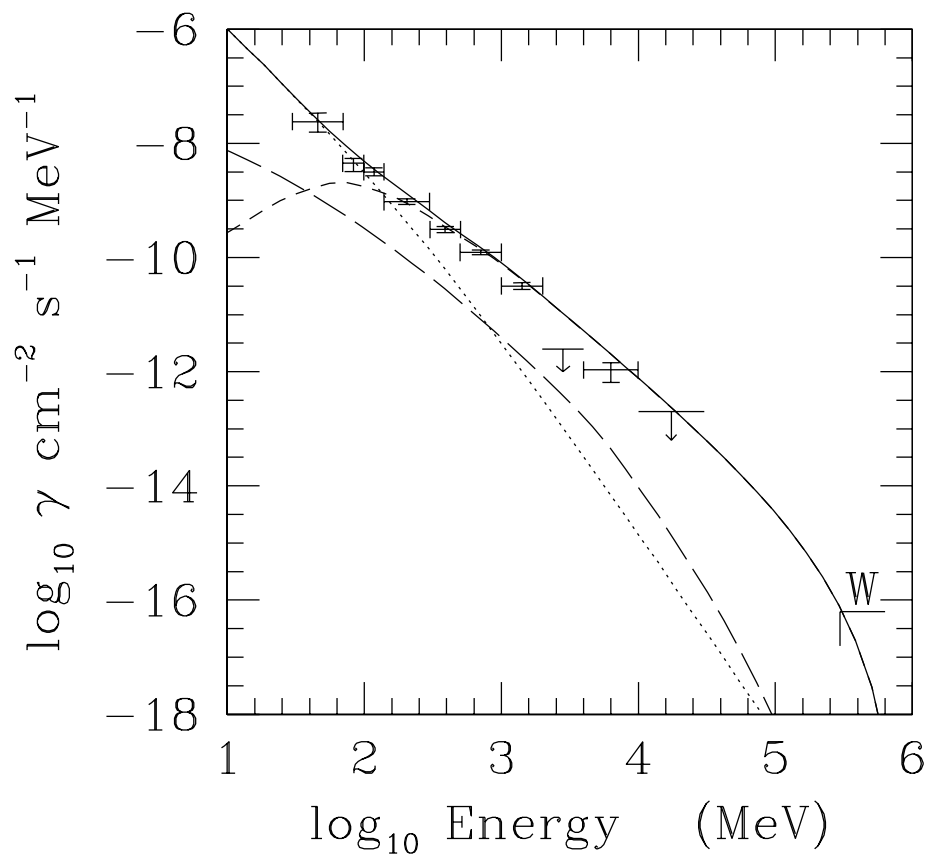


Fig. 9.— Same as Figure 8, but with $\alpha_e = 3.4$ above 10 MeV.

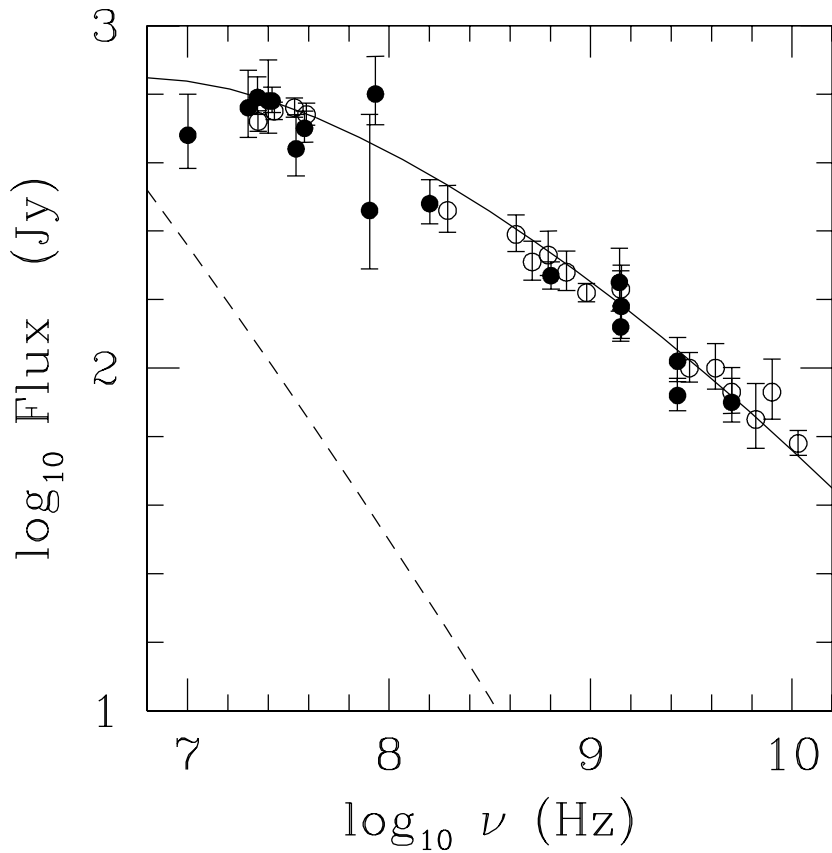


Fig. 10.— The synchrotron emission produced by the primary electrons (dashed curve) and secondary leptons (solid curves) associated with the γ -ray fits presented in Figure 9. The primary electrons are assumed to populate the same region as the secondary leptons, as a result of their diffusion (after cooling) from the dense cores.

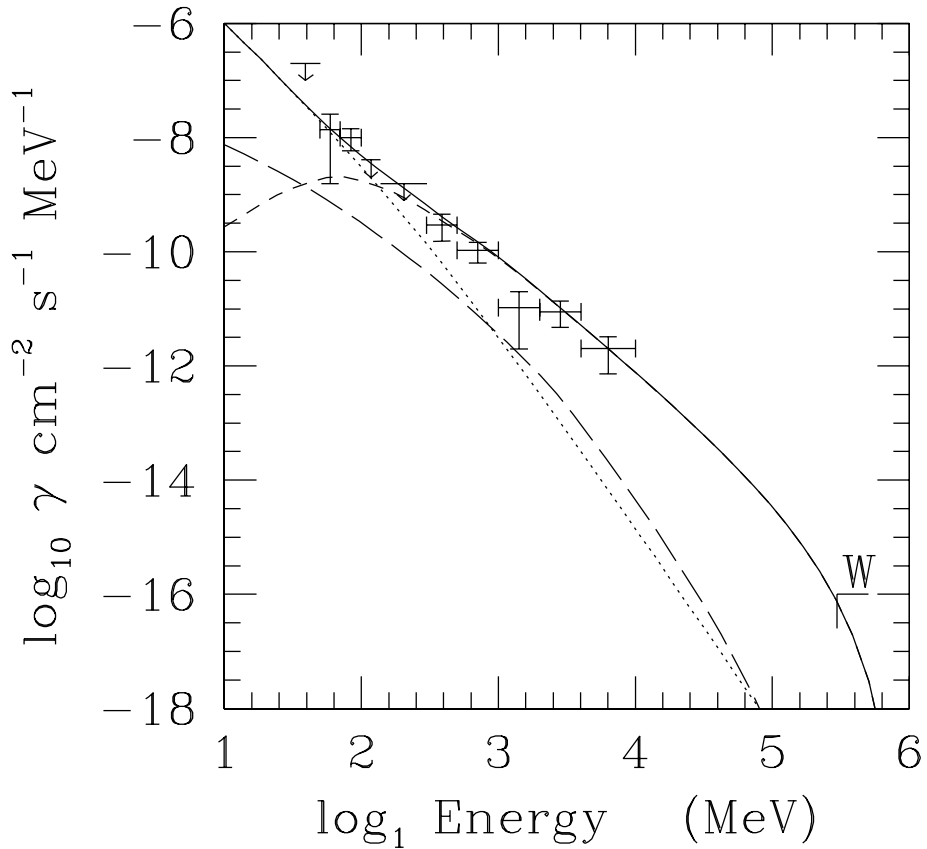


Fig. 11.— The γ -ray spectrum produced by the two-zone model applied to W44, where $\alpha_p = 2$ and $B = 0.43$ mG. Short dashed curve: neutral-pion decay emissivity; long-dashed curve: bremsstrahlung emissivity produced by secondary leptons; dotted curve: bremsstrahlung produced by primary electrons; solid line: total γ -ray emissivity. Data are taken from Merck et al. (1996) and Buckley et al. (1998).

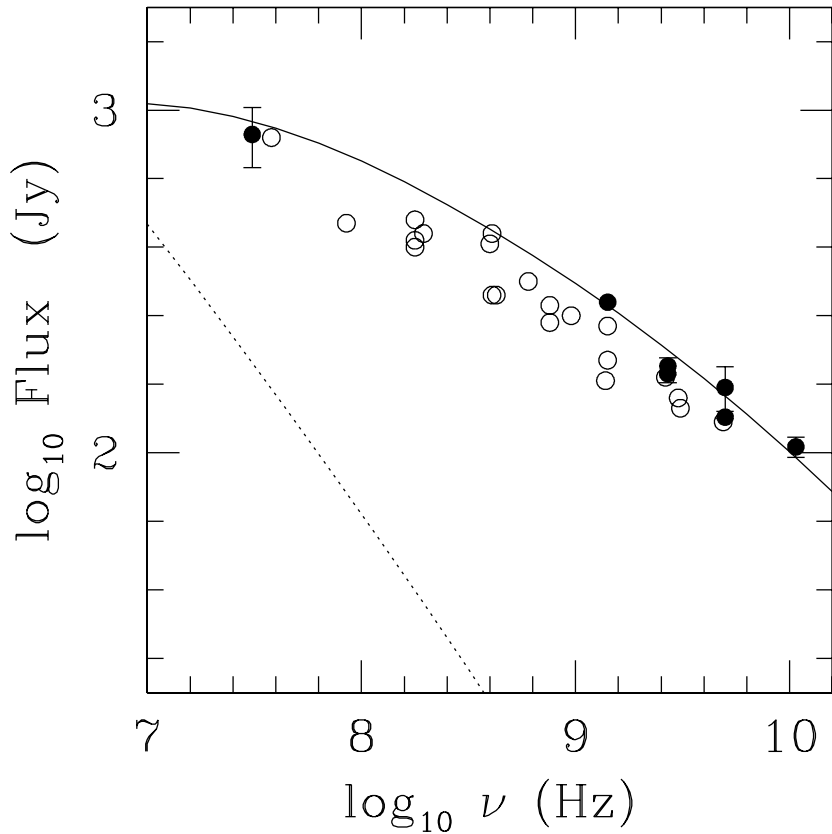


Fig. 12.— The radio spectrum produced by the two-zone model applied to W44, where $\alpha_p = 2$ and $B = 0.43$ mG. Dashed curve: synchrotron emission produced by the primary electrons that have diffused out into the shell; solid curve: synchrotron emission produced by the secondary leptons. Radio data taken from Kassim (1989). Solid circles represent data for which an error was quoted. Open circles represent data for which no error was quoted.

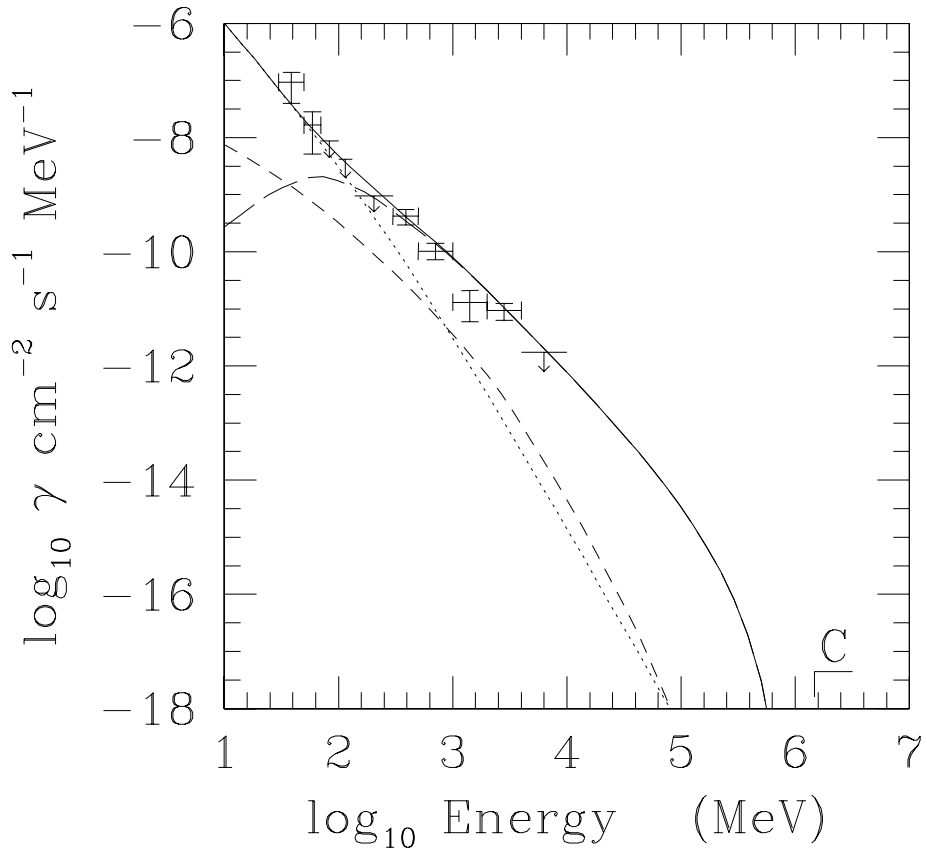


Fig. 13.— The γ -ray spectrum produced by the two-zone model applied to W28, where $\alpha_p = 2$ and $B = 0.43$ mG. Short dashed curve: neutral-pion decay emissivity; long-dashed curve: bremsstrahlung emissivity produced by secondary leptons; dotted curve: bremsstrahlung produced by primary electrons; solid line: total γ -ray emissivity. Data are taken from Merck et al. (1996) and Rowell et al. (2000).

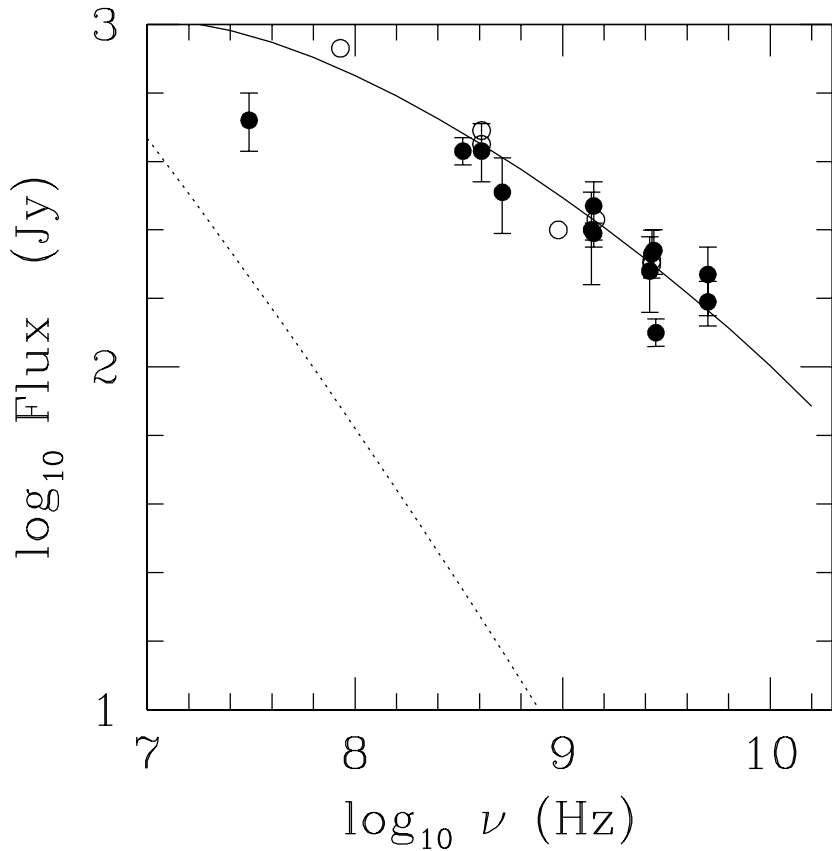


Fig. 14.— The radio spectrum produced by the two-zone model applied to W28, where $\alpha_p = 2$ and $B = 0.43$ mG. Dashed curve: synchrotron emission produced by the primary electrons that have diffused out into the shell; solid curve: synchrotron emission produced by the secondary leptons. Radio data taken from Kassim (1989). Solid circles represent data for which an error was quoted. Open circles represent data for which no error was quoted.

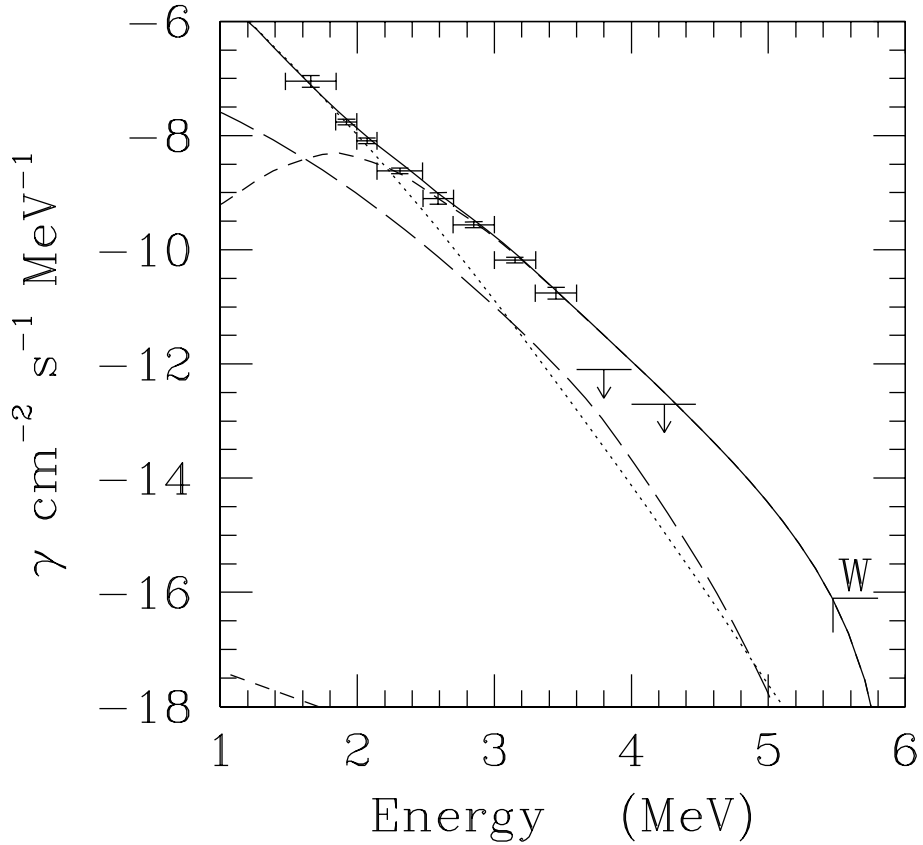


Fig. 15.— The γ -ray spectrum produced by the two-zone model applied to γ -Cygni, where $\alpha_p = 2.2$ and $B = 0.28$ mG. Short dashed curve: neutral-pion decay emissivity; long-dashed curve: bremsstrahlung emissivity produced by secondary leptons; dotted curve: bremsstrahlung produced by primary electrons; solid line: total γ -ray emissivity. Data are taken from Merck et al. (1996) and Buckley et al. 1998.

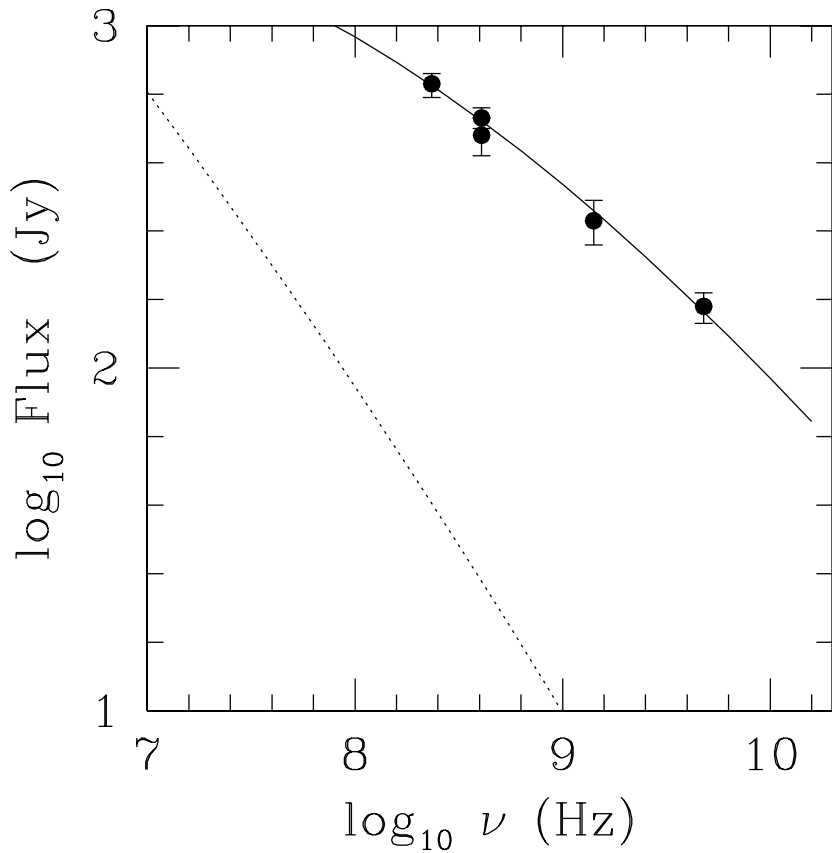


Fig. 16.— The radio spectrum produced by the two-zone model applied to γ -Cygni, where $\alpha_p = 2.2$ and $B = 0.28$ mG. Dashed curve: synchrotron emission produced by the primary electrons that have diffused out into the shell; solid curve: synchrotron emission produced by the secondary leptons. Radio data taken from Zhang et al. (1997).